Eur. Phys. J. A (2021) 57:99
https://doi.org/10.1140/epja/s10050-021-00412-z

THE EUROPEAN PHYSICAL JOURNAL A

Regular Article - Experimental Physics

Coupled channels effects in heavy ion reactions

A. Lépine-Szily[a], **R. Lichtenthäler**

Instituto de Fisica, Universidade de São Paulo, São Paulo, Brazil

Received: 27 December 2020 / Accepted: 18 February 2021 / Published online: 22 March 2021

Communicated by Nicolas Alamanos

Abstract The ECIS (Equations Couplées Itérations Séquentielles) code of Jacques Raynal continues to have an important role since its first version in the seventies. Its use to describe the elastic and inelastic scattering of light heavy ions at energies close to the Coulomb barrier is the first topic of this paper. Nuclear reactions with weakly bound stable and radioactive projectiles are described in the second topic, where the projectiles breakup is not taken into account in ECIS and a more recent formalism called Continuum Discretized Coupled Channels (CDCC) calculations is applied to them. The second topic also contains some results that were obtained at the Radioactive Ion Beams in Brasil (RIBRAS) facility, with a radioactive 2n-halo ^{6}He beam on light, medium mass, and heavy targets.

1 Introduction

The coupled channels code ECIS was developed by Jacques Raynal in the early seventies. It has been improved and further refined during the active scientific life of Raynal. This article will describe some applications of ECIS in works realized by the authors several decades ago, followed by recent works where ECIS could no longer be used since it does not allow the coupling to breakup channels, in the continuum. In noway pretends to be complete since the length limit does not allow and intends to be a homage to Jacques Raynal, known by one of the authors (ALSz).

ECIS was initially used mainly to perform coupled channels calculations for elastic and inelastic scattering cross sections measured with light or heavy projectiles, i.e Ref. [1]. A typical example of its early use (ECIS-73) [2] will be presented in Sect. 2. It was the elastic, inelastic and transfer reaction study of ^{16}O + ^{116}Sn system [3] measured at the Tandem Accelerator of CEA-Saclay, DPhN-BE, in 1974. In case of low energy, heavy ion nuclear reactions the Coulomb interaction extends to large distances, and the calculations demand integration up to very large radii and high number of partial waves. Using the ECIS conveniently modified in 1981 with Coulomb corrections [4] the radii necessary to attain convergence in the calculations, were considerably reduced [5].

Another measurement with the use of ECIS described in Sect. 2 was performed in the nineties using the beams of the 8UD Pelletron Tandem installed in the Open Laboratory of Nuclear Physics (LAFN, acronym in Portuguese) of the Institute of Physics of the University of São Paulo (IF-USP) in São Paulo, Brazil. It was the study of the elastic and inelastic scattering of the ^{12}C + ^{24}Mg system [6], where an interesting Q-dependence was found. The very inelastic, orbiting features of the ^{16}O+^{28}Si system, measured at the TANDAR Laboratory at CNEA, Buenos Aires, Argentina, were reproduced through the coupling of 35 inelastic and transfer channels to the elastic channel using ECIS88 [7].

ECIS was also used to analyze experiments on elastic and inelastic scattering and on the excitation of Giant Resonances at intermediate energies using proton, α-particle and heavy ion beams e.g. Refs. [8–11]. For low energy ($\leq$ 5AMeV) Coulomb excitation studies, with target excitation below the Coulomb barrier, one was on the safe side and could neglect the nuclear interaction. When the Coulomb excitation measurements of radioactive projectiles at intermediate energies became reality [12,13], the ECIS code was largely used to determine the very forward angular region where the nuclear interaction was negligible compared to the Coulomb.

In 1988 Jacques Raynal presented the ECIS88 version, at the "Workshop on applied nuclear theory and nuclear model calculations for nuclear technology applications"; Trieste Italy; 15 Feb–19 Mar 1988, announcing that he included in ECIS a statistical model part based on ANLECIS, developed by Moldauer [15,16]. The fusion barrier distributions obtained from quasi elastic excitation functions often took

[a] e-mail: alinka@if.usp.br (corresponding author)

advantage of the coupled channels quasi elastic and fusion calculations of ECIS [17]. ECIS has been used also to calculate the sub-barrier fusion cross section of ^{4}He and the two-neutron halo radioactive ^{6}He on ^{238}U, measured by detecting the fission fragments of the highly excited Pu compound nucleus [18]. The ECIS calculations reproduced well the cross sections above the Coulomb barrier, without taking into account the possible break up of ^{6}He. Later on, in 2004, the data indicating the sub-barrier enhancement reported in this work on fusion with ^{6}He were assigned to the two neutron transfer reaction instead of the fusion process [19].

ECIS is largely used even today to calculate nuclear data for reactors, mainly consisting in neutron scattering cross sections [20], as for ^{23}Na [21], the cooling material in fast reactors at CEA, Cadarache, France. Another application of ECIS is in the calculation of atomic displacement cross sections of materials due to energetic neutrons (from MeV up to 10GeV) [22]. This is an important parameter for the radiation damage rate in nuclear facilities, including fission and fusion reactors, accelerators and spallation sources. ECIS is used to calculate recoil energy distributions of atoms after the neutron elastic scattering. In Sect. 2, the applications of ECIS to elastic and inelastic scattering of low energy stable heavy ion beams is described. In Sect. 3, the measurements performed at the Radioactive Ion Beams in Brasil (RIBRAS) facility are presented.

2 Elastic and inelastic scattering of low and intermediate energy heavy ion beams

2.1 Elastic and inelastic scattering of ^{16}O +^{116}Sn

The elastic, inelastic and transfer reactions of the ^{16}O +^{116}Sn system [3] have been measured at the tandem accelerator of CEA-Saclay, DPhN-BE, in 1974, where one of the authors (ALSz) was on a post-doctoral appointment, working in the group of Mme Monique Conjeaud and M. Samuel Harar. She became responsible for the analysis of the ^{16}O +^{116}Sn data. The incident energy of the beam was 64 MeV and the detected ejectiles were ^{16}O, ^{15}N,^{14}C, and ^{12}C, corresponding to elastic, inelastic scattering, one-proton, two-proton, and α transfer reactions. Angular distributions were measured between Θ_{lab}=19 and 140^{o}. The energy spectra of the ^{16}O showed clearly the elastic peak and peaks corresponding to the excitation of the 2^{+} and 3^{-} states of ^{116}Sn at 1.283 and 2.266 MeV with a shoulder on the 3^{-} peak corresponding to unresolved higher excited states of ^{116}Sn. We were able to obtain the forward angle data of the inelastic peaks by subtracting the contribution of the small quantities of contaminant elements in the target, measured at backward angles with a low energy ^{16}O beam.

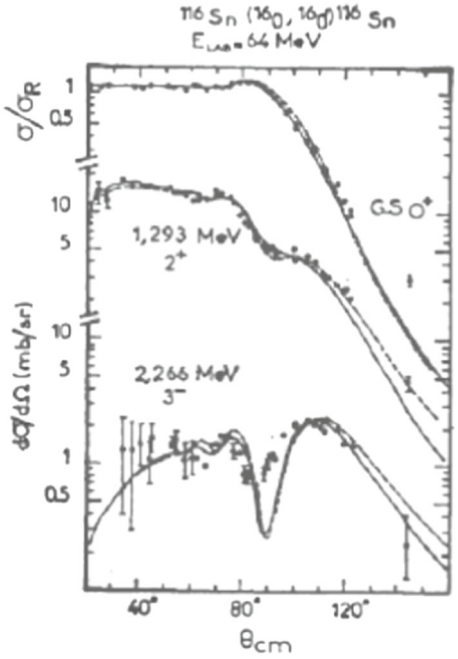

Fig. 1 Angular distributions of the elastic and inelastic scattering of ^{16}O on ^{116}Sn. The solid curves are results of coupled channels calculations and the dashed curves are results of DWBA calculations. Taken from Ref. [3]

To perform the cross section calculations for the elastic, and inelastic channels the coupled channels ECIS code was chosen and it was recomended that ALSz visit Jacques Raynal at Orme de Merisier, where the nuclear theory department of Saclay was installed. Jacques Raynal was a man of few words and these few words disappeared in his moustache and beard. Usually he had a pipe in his mouth not words. He preferred to speak French and the French of ALSz was far from being perfect so she had a great difficulty to communicate with him. But he was a very kind person with infinite patience and after several visits they could exchange ideas about details and results of the calculations. After some time she even learned that she had earned a reputation as someone who could communicate well with M. Raynal.

The angular distributions of the elastic and inelastic scattering are presented on Fig. 1; in the case of the 2^{+} and the 3^{-} states, they show clearly a dip which is due to interference between the Coulomb and nuclear excitation. The optical potentials for the elastic scattering had a Woods-Saxon shape with volume absorption. The form factors were given by the usual macroscopic description. The angular distributions of Fig. 1 for the 0^{+}, 2^{+} and 3^{-} states have been analysed simultaneously with ECIS, which allows a coupled-channel calculation for elastic and inelastic scattering. This code includes the possibility for a least-squares search on optical model and deformation parameters, which minimizes the χ^{2} value on both the elastic and inelastic data. The solid curves in Fig. 1

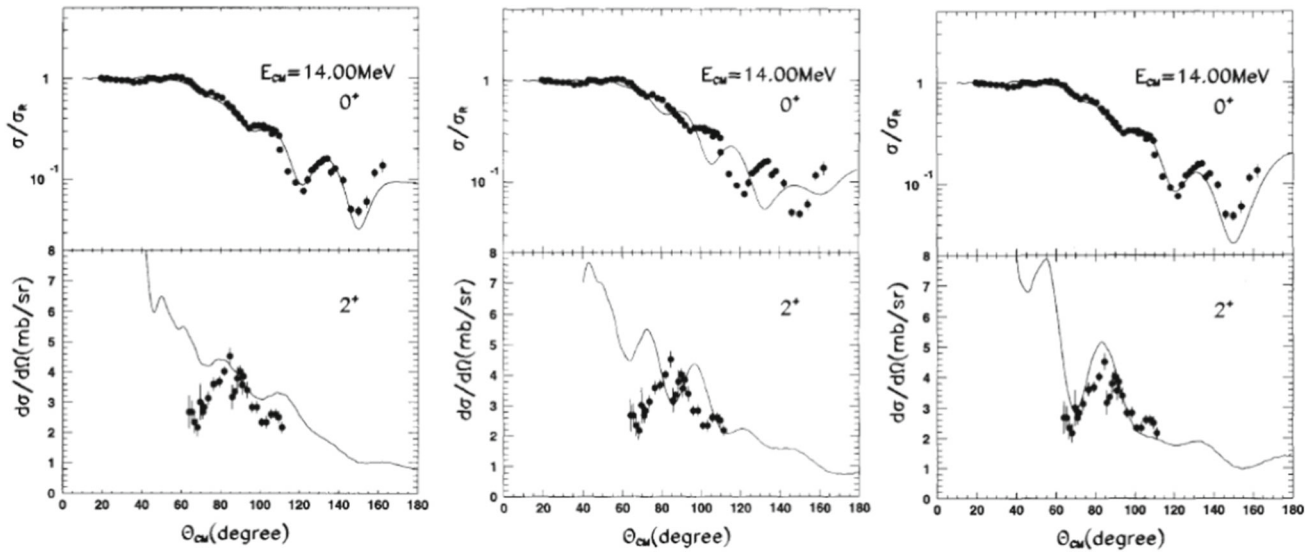

Fig. 2 Left panel: Elastic and inelastic (2^+) angular distributions fitted with coupled-channels calculations, using the rotational model and 0^+ - 2^+ coupling for E_{cm} = 14.00 MeV. Central panel: Coupled-channels calculations with 0^+ - 2^+ - 4^+ coupling and assuming the same optical potential in the incoming and outgoing channels (neglect Q-dependence) for E_{cm} = 14.00 MeV, as in the left panel. Right panel: Coupled-channels calculations with 0^+ - 2^+ - 4^+ coupling and taking into account the Q-value of the final states in the energy dependence of the optical potentials for E_{cm} = 14.00 MeV. Taken from Ref. [6]

are the results of one of the best fits, obtained when varying the real and imaginary well depths (V, W), the real diffuseness and the Coulomb and nuclear deformations of the 3^- state. The difficulty in reproducing the dip in the 3^- angular distribution was the topic of several discussions with M. Raynal. These calculations have been executed by including up to 200 partial waves and the integration was performed up to 39 fm. However, the increase in these values did not modify significantly the results in the angular range studied. As the calculations took many hours, ALSz left the boxes with the program at the end of the day and went to find the results in the morning of the next day. The post-doctoral appointment was nearing its end and she left Saclay before finishing the calculations. She was allowed to take the code with her to install on the most powerful computer of the USP. She had the help of M. Raynal until she finished the work. They exchanged letters and new versions of ECIS were at her disposal later on. Jacques Raynal was a great physicist, with a very broad culture and knowledge in nuclear physics but also a perfect gentleman, distant, but kind, patient, ready to help.

2.2 Study of the elastic and inelastic scattering of the ^{12}C+^{24}Mg system

The fifteen elastic angular distributions of the ^{12}C+^{24}Mg system measured at LAFN at energies around the Coulomb barrier present strong oscillations even at the lowest energy [6,23–25]. These oscillations could be reproduced with optical potentials that are very transparent not only on the surface but also in the nuclear interior, with $W_o/V_o \leq 0.01 - 0.02$ and notch tests realized at different energies show that the sensitivity to the potential values is not just on the surface but on an extended region from 2 to 8 fm. The ^{24}Mg nucleus is a strongly deformed prolate nucleus and the coupling of the inelastic excitations to the elastic channel can affect the elastic cross-section. We have performed coupled-channels calculations in the context of the rotational model in order to include this coupling [6]. These calculations have been performed using the code ECIS88 [26], assuming a deformed target nucleus and rotational model excitation form factors.

The energy variation of the potential volume integrals obeys the Threshold Anomaly [27] and is well reproduced by the dispersion relation calculations. The rapid energy dependence of the potentials close to the Coulomb barrier ($V_{CB} \sim$ 11 MeV) was presenting in a remarkable effect in the coupled channels calculations performed with the ECIS code.

In Fig. 2 three panels are presented; in the left panel the elastic and the 2^+ inelastic angular distributions were fitted with coupled channels calculations using the rotational model and 0^+ - 2^+ coupling. The best fit optical potentials for 14.00 MeV are used in the incoming (ground state) and for the exit channel (excited 2^+ state). The poor agreement for the inelastic angular distribution could not be improved with reasonable variation of the parameters. To improve the 2^+ result, the 4^+ excited state of the ^{24}Mg at E^* = 4.12 MeV was included in the coupled channels rotational model calculation. It was assumed as a pure rotational band state with the same quadrupole deformation parameter β_2 for the 0^+–2^+

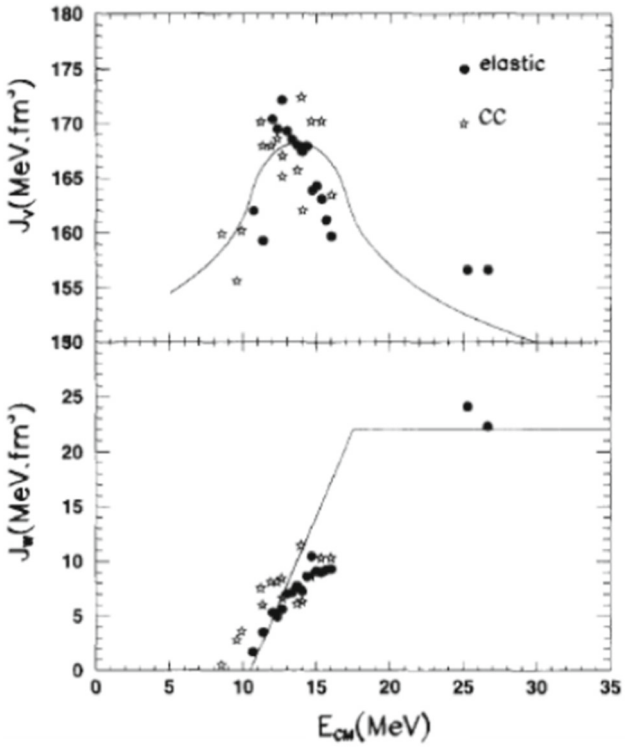

Fig. 3 Volume integrals of the best fit optical potentials used for the elastic scattering (dots) and for the final excited channels in the coupled channels calculations (stars) as a function of $E_{cm} - Q$. The solid curve is the dispersion relation calculation. Taken from Ref. [6]

and 2^+–4^+ transitions and with no direct excitation from the ground state.

The inclusion of the 4^+ state produced a strong shift in the calculated angular oscillations, as well as for the elastic and for the inelastic 2^+ scattering (see central panel of Fig. 2), when the same optical potentials were used in the incoming (ground state) and outgoing (2^+ and 4^+ states) channels. Using the same optical potentials in all of the channels implies not taking into account the Q-value of the outgoing channels in the energy dependence of the optical potentials. In this case, the optical potential to be used in the outgoing channel (with Q $\neq$ 0) is the one corresponding to the energy $E_{cm} - Q$. When the Q-value of the outgoing channels was taken into account in the energy dependence of the optical potential, that is, Q = 1.37 MeV was subtracted from the energy for the 2^+ state and Q = 4.12 MeV was subtracted from the energy for the 4^+ state, the calculated oscillations were again in good agreement with the experimental data (see right panel of Fig. 2). Using these values as starting point, the inelastic and elastic angular distributions were fitted allowing variations in the optical potentials of the excited channels. The panel on the right side of Fig. 2 shows the result of this calculation.

In Fig. 3, the energy variation of the potential volume integrals including results obtained by the coupled channels calculations fit procedures are presented. It obeys the Threshold Anomaly [27] and is well reproduced by the dispersion relation calculations. The Q-value dependence was particularly strong for the angular distributions at E_{cm} = 14.00 MeV because it corresponds to the top of the bell shaped peak in the energy dependence of the real potential, as shown in Fig. 3.

2.3 Orbiting phenomena in the ^{16}O + ^{28}Si system at 107.5 and 139 MeV incident energies

The elastic scattering of light mass α-structured ions on α-structured targets, with $A_p + A_T < 60$, presents strong oscillations in the angular distributions with a large increase of the cross sections at backward angles, an effect called Anomalous Large Angle Scattering (ALAS). Its first observations and studies occurred 50 years ago. However, work continues on these intriguing effects. At higher energies these systems present strongly damped binary processes, with evidences of non-compound dinuclear orbiting mechanism. Heavier and non-α systems, which present strongly damped binary processes, are characterized as fusion-fission. The aim of this work [7] was to investigate the existence and nature of strongly damped binary processes in the ^{28}Si + ^{16}O system, which is one where the ALAS phenomena were first observed.

The measurements were performed with the ^{28}Si beam produced by the Tandar Accelerator (Tandar Laboratory, CNEA, Buenos Aires, Argentina) at bombarding energies of 107.5 and 139.0 MeV, hitting SiO_2 targets. The detection was performed with 2 Silicon PSD detectors, preceded by gas Δ E detectors, having independent mobility and working in kinematic coincidence. At the lower incident energy the most probable binary fragments in the experiment were ^{16}O (target) and ^{28}Si (beam), indicating a non-compound orbiting mechanism.

The Q-value integrated angular distributions of the ^{16}O detected without kinematic coincidence are presented in Fig. 4. One may observe that the free data (without kinematic coincidence) follow the $1/\sin\theta_{c.m.}$ behavior (dashed curves) at back angles, indicating a long lifetime. However, the angle-integrated cross sections of the ^{28}Si + ^{16}O decay channel are one order of magnitude higher than the binary cross sections of the ^{35}Cl + ^{12}C and ^{31}P + ^{16}O reactions at similar energies, which were shown to proceed through fusion-fission processes.

Many features of the ALAS effect, such as elastic, inelastic and α transfer angular distributions and excitation functions, were well reproduced by coupling the elastic channel to multi-step α-particles exchange processes [28–32]. In order to describe this complex situation, coupled-channels calculations were performed by taking into account all of the experimentally observed channels. Besides the resolved individual final states, the energy spectra were divided into bins of 1

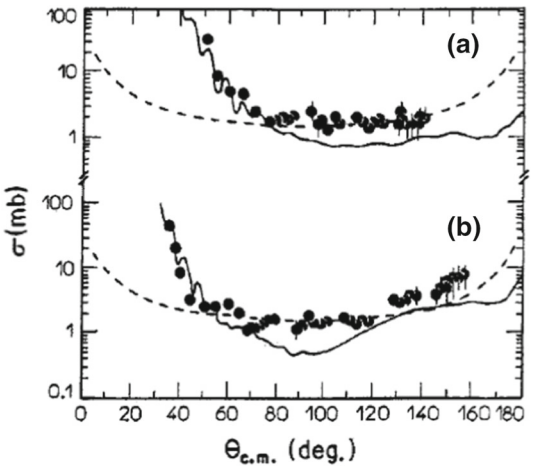

Fig. 4 **a** The Q-value-integrated angular distributions of ^{16}O nuclei, detected without kinematic coincidence at $E_{c.m.}$ = 39.1 MeV. The dashed line shows the 1/sin$\theta_{c.m.}$ behavior. The solid line is the result of coupled-channels calculations described in the text. **b** The Q-value-integrated angular distributions at $E_{c.m.}$ = 50.5 MeV. Taken from Ref. [7]

MeV in order to construct "experimental angular distributions"for these energy bins. Coupled-channels calculations were performed with 15 inelastic channels, and the outgoing systems ^{20}Ne+^{24}Mg* and ^{12}C+^{32}S* contribute, respectively, with 11 and 9 channels. The total number of channels included in the calculation were 33 and 35 for $E_{c.m.}$= 39.1 and 50.5 MeV, respectively. The inelastic excitations are assumed to be due to rotational quadrupole transitions in ^{28}Si, all with the same deformation parameter, and the transfer transitions are due to α-cluster transfers, all with the same spectroscopic amplitudes. All of the coupling possibilities between the different channels in the symmetric rotational model were included in the calculation. The code ECIS88 [26] was used which solves exactly the coupled-channels equations. The dynamics of the transfer reactions is treated in an approximate way in ECIS88, neglecting the recoil of the target nucleus and using a zero-range interaction. These approximations mainly affect the absolute value of the cross section and, to a lesser extent, its angular shape. We also used the same form factor for the nuclear inelastic excitation and transfer in order to simplify the calculation and to be able to couple more channels. The adopted Coulomb deformation parameter β_2^c of ^{28}Si was used and the nuclear deformation length was assumed to be equal to the charge deformation length.

The coupled-channels calculations were performed using the following strategy: initially, the ground state was coupled to a few excited states of known spin, using the starting optical potential [33] for the incoming and all outgoing channels and the adopted deformation length. By varying V, W, and β_2 , and keeping the geometry fixed, the calculation was required to fit the experimental angular distributions keeping the same optical potentials in all excited channels. As the fit improved, more channels were included, treating the spin also as a free parameter, until all of energy bins were included as channels. The potential depths were reduced by the fitting procedure as more and more channels were coupled and the opacity measured by W/V was reduced also. This reduction in the absorption is a consequence of the explicit inclusion of many reaction channels in the calculation. The nuclear deformation parameter also had to be reduced as more and more inelastic channels were coupled. These coupled-channels calculations reproduce fairly well the elastic and all of the inelastic angular distributions, even those with high excitation energy, including the intermediate angle and back-angle rise in the cross section.

The Q-value integrated cross section plotted in Fig. 4 as a solid curve was obtained by the sum of all calculated angular distributions of the 33 (35) channels. The overall agreement is remarkable, with respect to both the absolute value and the angular behavior. This calculation, treating simultaneously 35 channels and performing χ^2 minimization search on parameters for the total χ^2 of 35 channels was a "tour de force and only possible with the ECIS code. It has proved that the multi-step α-particles exchange process can explain not only the ALAS effect but also the strongly damped binary, non-compound orbiting effect, both manifested in n-α structured systems.

3 Coupled channels effects in direct reactions with stable and Radioactive Ion Beams (RIB)

Low energy nuclear physics went through an interesting historic evolution during the late seventies, eighties and nineties closely related to the evolution of computers and computer codes. By the end of the seventies and beginning of the eighties there were few computers and codes capable of performing calculations considering all of the required complexity of the nuclear models. Most of the available machines were mainframes, such as IBM-360 and Vax-780, which had small memory capacity and slow processors. In heavy ion collisions, the number of open reaction channels increases considerably as the bombarding energies overcome the Coulomb barrier. The Optical Model is the simplest calculation to describe the elastic scattering and requires the numerical solution of the homogeneous Schroedinger equation using a complex scattering potential whose imaginary part takes into account the effect of all reaction channels. The numerical scattering wave function is a 2(Lmax + 1) × Nr matrix where Lmax is the maximum angular momentum involved in the collision and Nr is the number of r-steps in the integration. Usually, these numbers were large, typically of the order of Lmax = 20–100 and Nr = 200–2000 for the scattering of heavy ions at energies above the Coulomb bar-

rier. The description of non-elastic channels such as inelastic scattering and transfers was, at that time, a challenge. In a first approach, inelastic scattering and transfer calculations could be done in Distorted Wave Born Approximation (DWBA) which involves the numerical computation of a six-dimensional integral. It required the storage of the scattering wave functions in the entrance and exit channels, demanding a memory frequently unavailable. In order to perform such calculations, the computed scattering wave functions had to be written in the disk to be subsequently used in the DWBA integral computation, making the calculation very lengthy. In addition, Coulomb excitation (COULEX) is an important process in heavy ion collisions which, due to the long range of the Coulomb interaction, requires the use of a very large number of partial waves in the scattering amplitude and extended integration in r-space in order to reach convergence. Efficient methods have been developed to overcome this difficulty in the case of Coulex. However, at that time, few programs were able to perform 'exact' DWBA calculations. DWUCK4 [34], LOLA [35] and DWUCK5 [36] were examples of existing DWBA codes. DWUCK4 used two approximations (zero-range and no-recoil) to transform the six-dimensional integral into a three-dimension one saving memory and computing time. However, such approximations resulted very inaccurate in many cases. Mainly, for transfers involving more than one nucleon or clusters of nucleons such as alpha particles, zero-range and non-recoil approximations usually provided cross sections several orders of magnitude below the experimental ones. Finite range and recoil effects were incorporated in LOLA, DWUCK5 and Ptolemy [37] codes improving considerably the results and allowing the determination of reliable spectroscopic factors directly from transfer data. However, the situation was not so simple. In many cases, low energy scattering involves strong coupling between different reaction channels making the distorted wave Born approximation insufficient to describe the data. In these cases, coupled channels calculations are necessary and ECIS was, at some point, the only computer program capable of performing exact coupled channels calculations for the inelastic scattering. Solving the coupled channels problem for inelastic scattering is somewhat simpler than in the case of transfer reactions since the considered states are orthogonal by construction. For transfer reactions, non-orthogonality effects are important and not trivial to be included in the calculations. Chuck [38] and FRESCO [39] were the programs under development for Coupled reaction channels (CRC) calculations.

At low energies, coupled channels effects are important in many situations since the collision partners have time to exchange particles in several orders making the one-step DWBA insufficient to describe the data. Higher order effects reactions are nicely illustrated in low energy (d,n) and (d,p) reactions [40]. Single nucleon transfers such as (d,n) and (d,p) reaction are usually well described by DWBA but, at very low energies, higher order coupled channels effects play an important role.

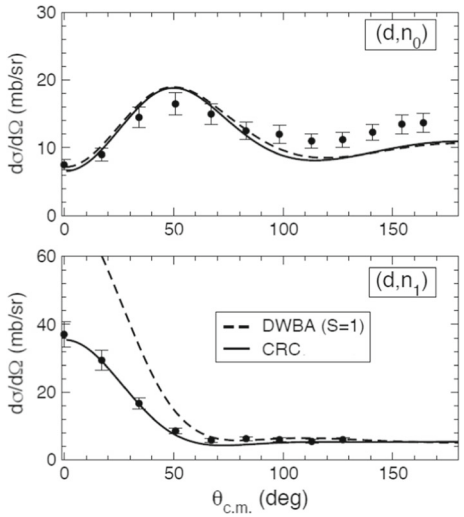

Fig. 5 Angular distributions of the ^{16}O(d,n)^{17}F and ^{16}O(d,n1)^{17}F* reactions at $E_d = 2.85$ MeV. Figure taken from [40]

In Fig. 5 we show the angular distributions of the ^{16}O(d,n)^{17}F reaction leading to the gs (d,n_0) and to the first excited state of ^{17}F (d,n_1) [40]. ^{17}F is an exotic proton rich nucleus which has only one excited s-state bound by only 105 keV. This is a typical proton halo state with low angular momentum ($l = 0$) and low binding energy for the breakup into $p+^{16}$O. DWBA calculations for the (d, $n1$) reaction (see Fig. 5 lower) give cross sections considerably larger than the data, resulting in spectroscopic factors for $< 16O|17F >$ below unity (SF = 0.7−0.85), considerably smaller than expected. As higher order effects were taken into account in a full coupled channel calculation the discrepancy was solved and SF = 0.96(12) was obtained showing that such higher order coupled channels calculations are necessary to explain the data and provide reliable spectroscopic factors at these low energy reactions.

During the eighties, the advent of higher energy laboratories such as GANIL, MSU, GSI moved nuclear physics to the unexplored realm of intermediate energies. Reactions such as multi-fragmentation were discovered and new models were developed to describe such reactions making the low energy nuclear models more and more obsolete. On the other hand, the possibility of producing secondary beams of nuclei out of the stability valley opened the possibility to explore the new research field of exotic nuclei. Secondary beams of exotic nuclei were usually produced by the in-flight method using fragmentation reactions at intermediate energies. In the in-flight method, the energy of the secondary beam is directly related to the primary beam energy and, as the primary beams usually had high energies (tens to hundreds of

MeV per nucleon), the secondary beams were also produced in this energy region.

The production in laboratory of unstable and exotic nuclides during the period 1980–1990 increased the size of the nuclear chart from about 1200 known nuclides in 1960 to about 3000–4000 nowadays. The ^{11}Li isotope was probably the most important event in the 1985 by Tanihata [41]. ^{11}Li presents extremely unusual properties such as a very large total reaction cross section and a pronounced neutron halo with two loosely bound neutrons forming Borromean three-body structure [41]. The ^{11}Li neutron halo was nicely probed by measuring the ^{9}Li transversal momentum distribution in a breakup experiment at 600 MeV/n [42].

Exotic nuclei such as ^{6}He, ^{11}Li, ^{11}Be, up to very neutron rich species such as ^{22}C, ^{24}O and ^{32}Mg and up to heavier nuclei have been produced in laboratory allowing nuclear structure studies near the drip lines. New interesting phenomena such as modifications in the nuclear shell structure, the quenching of the shell model energy gaps and new magic numbers have been discovered, with consequences in the astrophysics, in particular in the nucleo-synthesis of elements heavier than iron.

At the same time, Isotope on-line Separation (ISOL) techniques, under development during the eighties and nineties, allowed the production of secondary beams with properties as good as the primary beams. In this method, the exotic nuclei are produced by fragmentation reactions in thick targets, designed to support high power primary beams. The nuclei produced by fragmentation reactions in the primary target diffuse through the hot target matter all the way up to an ion source to be re-ionized and re-injected in a secondary accelerator [43], allowed the production of low energy radioactive ion beams.

In the nineties, laboratories such as Rex-Isolde in Cern, Louvain-la-Neuve in Belgium and TwinSol at Notre Dame University (EUA) [43,44] were starting to produce low energy RIB using both ISOL and in-flight methods, causing a revival of the low energy nuclear physics, now with secondary beams of exotic nuclei. Due to the very small breakup energies of some of these exotic projectiles, reactions such as breakup/transfers seem to play a very important role in the scattering process and the coupling between the ground state and the continuum became an essential ingredient to understand the physics of the collision with exotic projectiles.

The seminal review paper of Austern and collaborators published in 1987 [45], gathered the progresses and results of previous attempts to present the formalism of a three-body coupled channels calculation of the collision between the deuteron and a heavy target, which takes into account the breakup of the deuteron. The weakly bound deuteron is described by its bound, ground state plus the pn scattering states, which are labelled by their continuous and unbounded momenta **k**. This extended set is discretized and truncated to allow the finite coupled-channels analysis of the deuteron-nucleus system and the method was denominated "Continuum Discretized Coupled Channels" (CDCC) calculation. Apparently Jacques Raynal was familiar with the subject of continuum discretization, but he did not introduce this formalism in ECIS. Thus, the subject which nowadays attracts a lot of attention unfortunately cannot be treated by ECIS. We will describe shortly how the analysis of direct reactions using coupled channel calculations has evolved with the inclusion of the breakup channel. This description will not be complete, some works and studies are quoted and also the available review articles. The effect of the breakup on fusion reactions is also out of the scope of this work.

In the very beginning of the nineties the new formalism began to be used to analyze elastic scattering data of weakly bound, stable nuclei as deuterons and ^{6,7}Li on different targets, ranging from ^{4}He, through ^{12}C, ^{28}Si, ^{58}Ni, ^{120}Sn, up to ^{208}Pb at energies ranging from 6 Mev/n up to 100 MeV/n [46–48]. Several conclusions could be obtained, as the dominance of Coulomb breakup at near barrier energies and heavy targets, the decrease of the importance of continuum coupling with increasing incident energy, however the nuclear breakup at forward angles increases with energy and becomes comparable to the Coulomb breakup, which dominates at low energies.

At near barrier energies the exclusive breakup of ^{6}Li on ^{208}Pb [49] and on ^{28}Si [50,51] was measured and reproduced by CDCC calculations. The inclusive α-particle production was much larger, suggesting other mechanism, as the "stripping breakup", where the deuteron or just one neutron are captured by the target. Several measurements were realized on Z = 13,14 targets to observe the coupling effects at much lower Coulomb interaction. The barrier distributions extracted from back-angle, near and sub-barrier, quasi-elastic excitation functions of ^{6}Li and ^{7}Li on ^{28}Si [52] indicated strong continuum coupling only for ^{6}Li. Performing CDCC and CRC calculations for the breakup and for the one neutron stripping the intriguing conclusion was the following: the transfer presents large cross section but small coupling effect on the elastic scattering, while the breakup cross section is small but the coupling to the continuum has strong influence on the elastic scattering. The ^{6}He + ^{27}Al elastic scattering [53] measured at the Brazilian radioactive beam facility RIBRAS [54] at near-barrier energies was well reproduced by standard optical model calculations using the double-folding São Paulo Potential (SPP) [55], and the total reaction cross section was similar to stable weakly-bound nuclei on ^{27}Al. This suggested the absence of continuum coupling. The Coulomb breakup is much reduced due to the low Z of the target, and the nuclear breakup should be more effective at backward angles (150 and 170^{o}) as indicated in Ref. [52].

The coupling to the breakup at intermediate energies also produced noticeable effect on the elastic scattering at very forward angles, using radioactive halo projectiles as ^{6}He, ^{11}Be on ^{12}C [57,58]. The coupling to the breakup was simulated adding a complex Dynamic Polarization Potential (DPP) [59], with a repulsive real part on the surface and a weak imaginary part. However, the effect is much stronger at incident energies close to the Coulomb barrier, and thus most of the subsequent works were realized using exotic low energy beams. A review article published in 2009 [60] gives a very complete panorama of the activity up to this date.

The elastic scattering at near barrier energies of neutron halo projectiles on heavy targets was measured at several laboratories around the world. The Fresnel peak suppression is a typical effect observed in these measurements [61–68] and arises from the strong projectile dipole polarizability in the Coulomb field of the target leading to the projectile breakup. Coulomb breakup occurs even for large partial waves introducing a long range absorption which will show its effect at forward angles, in the Fresnel peak angular region. A similar effect has been previously observed in stable nuclei elastic and inelastic scattering due to the excitation of low lying states in the target [69,70]. The excitation of states near the ground state seems to be the common process in both cases, the breakup for loosely bound projectiles and the long range inelastic Coulomb excitation for heavy nuclei, both producing a similar Fresnel peak damping in the elastic scattering distributions.

In the collision of ^{6}He with heavy targets a large production of α-particles was observed, however its cross section is much underestimated by the direct breakup calculations indicating the importance of neutron transfer to the target nucleus [71–74]. The inclusive breakup at near barrier energies was measured for the 2 neutron halo Borromean ^{11}Li projectile on a ^{208}Pb target. The breakup probability was reproduced by four-body CDCC calculations with nuclear and Coulomb coupling [75]. The breakup of the exotic proton-halo ^{8}B on ^{58}Ni target was measured [76] and its angular distribution was well explained by Coulomb and nuclear breakup three-body CDCC calculations [77]. In the three-body CDCC description of the collision of a three body, exotic projectile (two neutron halo + core) with a target, the two neutrons are supposed to form a dineutron cluster. A more exact, four-body description of the collision was developed [78–80] and it gives better agreement with the experimental data.

Computer programs such as FRESCO were developed to perform continuum discretized coupled channels calculations (CDCC) taking into account the effect of the continuum. The advent of personal computers with large memory capabilities and fast processors allow the computation of scattering amplitudes considering the coupling to a large number of reaction channels, considering the spin of the nuclei, in an excitation energy region involving bound and unbound states of the colliding partners, a task which was unthinkable 10 years ago.

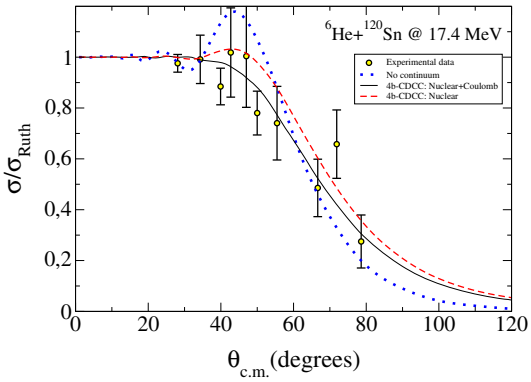

Fig. 6 ^{6}He+^{120}Sn elastic scattering distribution. Taken from [83]

In 2004 Radioactive Ion Beams in Brasil (RIBRAS) [54,81,82] was installed in the nuclear physics department of the Institute of Physics of the University of São Paulo. RIBRAS consists of a double superconducting solenoid system to select secondary beams of light exotic nuclei produced in the collision between the 8UD-Pelletron tandem primary beam and a thin primary target. At these low primary beam energies (3-5 MeV/n) nucleon transfer reactions such as ^{9}Be(^{7}Li,^{6}He), ^{9}Be(^{7}Li,^{8}Li) produce exotic nuclei such as ^{6}He, ^{8}Li, ^{7}Be, ^{8}B and others with secondary beam intensities from 10^{3} to 10^{6} pps [54,81,82].

Since the RIBRAS inauguration an extensive low energy RIB experimental program has been carried out. Elastic scattering and reactions induced by light exotic nuclei on several targets have been measured. Elastic scattering angular distributions of ^{6}He on light ^{9}Be, medium mass ^{27}Al, ^{58}Ni and heavy targets ^{120}Sn allow the study of the interplay between Coulomb and nuclear interactions. The Fresnel peak damping has been observed in the ^{6}He+^{120}Sn elastic scattering angular distributions when compared to OM and 3 and 4-body CDCC calculations [83] (see Fig. 6).

A systematic study of total reaction cross sections obtained from the elastic scattering angular distributions [53,83,85–87] analysed by Optical model and Continuum Discretized Coupled Channels calculations has been performed comparing strongly bound, weakly bound stable and exotic nuclei systems. To compare the reaction cross section of different systems at different energies transformation are performed which account for the geometrical effect in the cross section due to the size of the system and the effect of the Coulomb barrier with respect to the energy [88].

The comparison of systems with strongly bound, weakly bound stable and exotic projectiles has shown an interesting behavior (see Fig. 7), Such studies indicate that, for ^{6}He projectiles, the reduced total reactions cross sections [90,91] are systematically larger than the ones for weakly bound stable

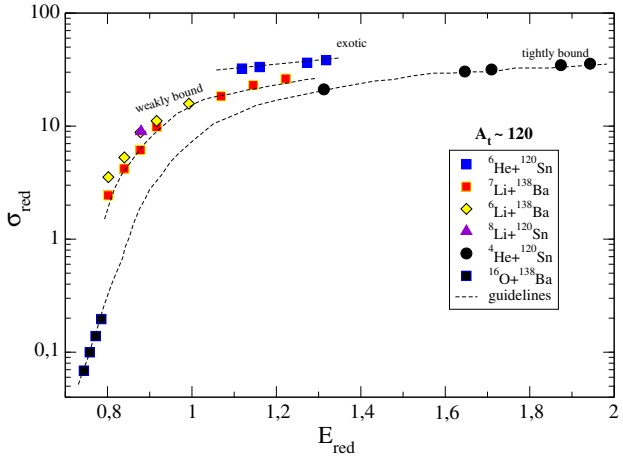

Fig. 7 ^{6}He+^{120}Sn reduced total reaction cross-section compared to systems with target mass around A=120. Taken from [83]

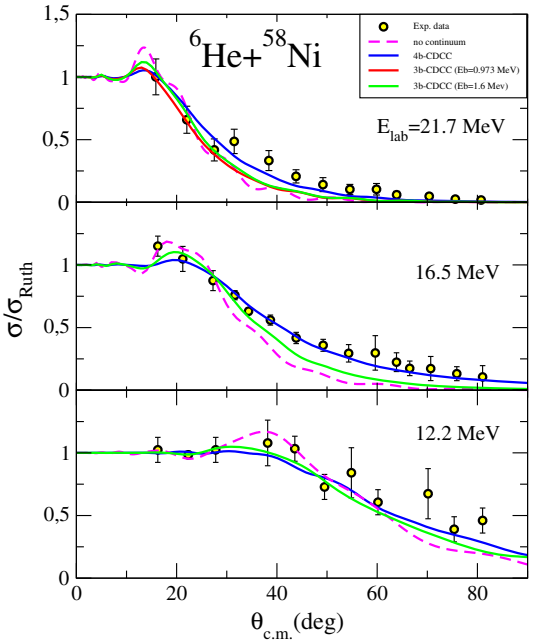

Fig. 8 ^{6}He+^{58}Ni angular distributions [92] compared with 4b and 3b-CDCC calculations. Figure taken from Ref. [92]

nuclei which are larger than the strongly bound projectiles. This behavior is attributed to a larger radius of the halo nuclei and has been observed in several other systems using different reduction methods [82,86,89–91].

In Fig. 8, ^{6}He+^{58}Ni elastic angular distributions are presented which were very successfully reproduced by 4b-CDCC calculations [79,80,92], indicating that the ^{6}He plus target collision is a four-body collision process involving the two neutrons and the ^{6}He alpha projectile core plus the target.

The neutron halo signatures go beyond the elastic scattering and total reaction cross section. Low energy study of nuclear reactions induced by the ^{6}He projectile has shown

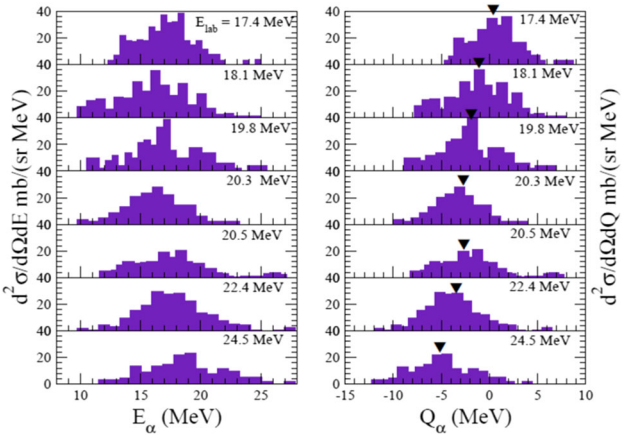

Fig. 9 Alpha particle energy distributions from the ^{6}He+^{120}Sn scattering [73] @60 deg. Arrows indicate the centroids of the distributions. Figure taken from ref. [73]

a large production of alpha particles in the collision with the ^{120}Sn target [72,73]. In a first approach, the projectile breakup could be considered as the principal reaction channel responsible for this high alpha particle yield. However, a deeper analysis has shown that 3-body and 4-body CDCC calculations, provided breakup cross sections several times smaller than the measured ones, indicating that mechanisms other than the elastic projectile breakup are taking place. In addition to the magnitude of the breakup cross sections, the measured alpha particle energy distributions are not explained by CDCC calculations as well. Direct breakup predicts a broader energy distribution centered at energies considerably smaller than the observations. The measured alpha particle energy distributions are in better agreement with Q-optimum predictions for neutron transfer reactions rather than direct projectile breakup predictions [19,72–74,93]. Indeed, DWBA calculations for the di-neutron transfer to continuum as in ^{120}Sn(^{6}He,α)^{122}Sn reaction provided results much more consistent with the observations either for the magnitude of the cross sections or for the energy distributions [72]. As the direct projectile breakup seems to be the main process at higher energies, at lower energies there are indications that the projectile interacts more strongly with the target, through a neutron transfer reaction, leaving the recoil nucleus in excited states.

In Fig. 9 we show the alpha particle energy distributions measured in the ^{6}He+^{120}Sn collision as a function of the ^{6}He bombarding energies [73]. In Fig. 9 (left) we plot the alpha particle energies as measured in the laboratory and, in the right, the same distributions with the energy axis transformed to the Q-value of the di-neutron ^{120}Sn(^{6}He,α)^{122}Sn* transfer. The ^{122}Sn excitation energy is adjusted to reproduce the measured alpha particle energies. This transformation shows that values around $Q_{reac} = 0$ are being populated at lower bombarding energies as predicted by simple linear and angu-

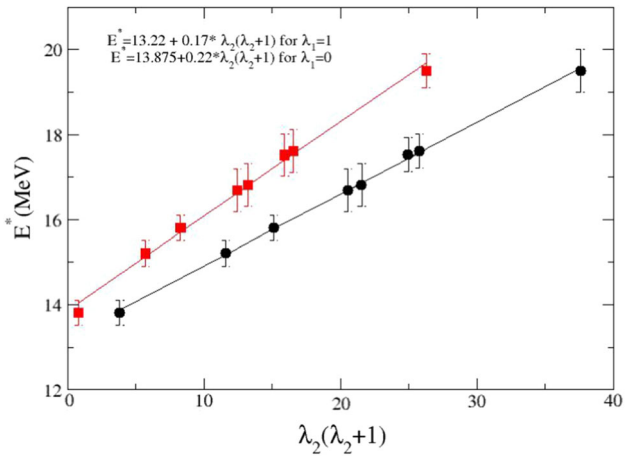

Fig. 10 Excitation energy of the recoil ^{122}Sn nucleus versus the square of the final angular momentum [73] for two different initial angular momenta (li=0 (red) and l_i=1 (black)) of the di-neutron in the ^{6}He projectile. Figure taken from [73]

lar momentum matching conditions for neutron transfers. As the bombarding energy increases the centroids of the energy distributions move to more and more negative Q-values corresponding to more and more excitation energy fed into the recoil nucleus. Q-optimum calculations using Brink's [94] formula show that this increasing excitation must be associated with an increase in the di-neutron orbital in the recoil ^{122}Sn system, forming a rotational-like band. In Fig. 10 we plot the excitation energy versus the square of the final orbital angular momentum for two different initial angular momenta ($\lambda_i = 0, 1$). The $\lambda_1 = 1$ case seems to provide a better agreement with the rotational model. The moment of inertia obtained from this rotational band is compatible with the expected value for the ^{120}Sn+2n system.

Acknowledgements We sincerely thank W. Seale for his very careful and judicious reading of the manuscript. This work has been partially supported by Conselho Nacional de Desenvolvimento Científico e Tecnológico – CNPq (Brazil) Grants no. 308935/2018-7, 301842/2019-1, Fundação de Amparo à Pesquisa do Estado de São Paulo, FAPESP (Brazil), contracts no. 2019/07767-1, 2019/02759-0, 2013/22100-7.

Data Availability Statement This manuscript has associated data in a data repository. [Authors' comment: The data of 12C+24Mg (ref.6) are deposited at http://www-nds.iaea.org/EXFOR/D0421 and the data of 16O+28Si (ref.7), at http://www-nds.iaea.org/EXFOR/D0541002. The data of 16O+116Sn (ref.3) are not deposited, please contact the corresponding author in case of interest. The RIBRAS data of 6He+120Sn (ref.72,73,83) and 6He+58Ni (ref.92) are deposited at http://nrv.jinr.ru/nrv/webnrv/elastic_scattering/reactions.php.].

References

1. A. Baeza, B. Bilwes, R. Bilwes, J. Diaz, J.L. Ferrero, J. Raynal, Nucl. Phys. A **437**, 93 (1985)
2. J. Raynal, Saclay Report No. DPh-T 69/42 (unpublished); and private communication (2019)
3. A. Lépine, C. Volant, M. Conjeaud, S. Harar, E.F. da Silveira, Nucl. Phys. A **289**, 187 (1977)
4. J. Raynal, Phys. Rev. C **23**, 2571 (1981)
5. N. Alamanos, Eur. Phys. J. A **56**, 212 (2020)
6. W. Sciani, A. Lépine-Szily, R. Lichtenthäler F., P. Fachini et al., Nucl. Phys. A **620**, 91 (1997)
7. J.M. Oliveira Jr., A. Lépine-Szily, A.C.C. Villari, R. Lichtenthäler et al., Phys. Rev. C **53**, 2926 (1996)
8. A. Sethi, N.M. Hintz, D.N. Mihailidis, A.M. Mack et al., Phys. Rev. C **44**, 700 (1991)
9. B. Bonin, N. Alamanos, B. Berthier, G. Bruge et al., Nucl. Phys. A **445**, 381 (1985)
10. J. Barrette, N. Alamanos, F. Auger, B. Fernandez et al., Phys. Lett. B **209**, 182 (1988)
11. S. Dubey, S. Mukherjee, D.C. Biswas, B.K. Nayak et al., Phys. Rev. C **89**, 014610 (2014)
12. T. Motobayashi, Y. Ikeda, Y. Ando, K. Ieki et al., Phys. Lett. B **346**, 9 (1995)
13. V. Chisté, A. Gillibert, A. Lépine-Szily, N. Alamanos et al., Phys. Lett. B **514**, 233 (2001)
14. J. Raynal, Coupled channel calculations and computer code ECIS. United States: World Scientific Pub Co. (https://inis.iaea.org/search/search.aspx?origunderscoreq=RN:23006204) (1989)
15. P.A. Moldauer, Phys. Rev. C **11**, 426 (1975)
16. P.A. Moldauer, Nucl. Phys. A **344**, 185 (1980)
17. H. Timmers, J.R. Leigh, M. Dasgupta, D.J. Hinde et al., Nucl. Phys. A **584**, 190 (1995)
18. M. Trotta, J.L. Sida, N. Alamanos, A. Andreyev et al., Phys. Rev. Lett. **84**, 2342 (2000)
19. R. Raabe, J.L. Sida, J.L. Charvet, N. Alamanos et al., Nature **431**, 823 (2004)
20. B.V. Carlson, Optical model calculations with the code ECIS95 (INIS-XA–858). Gandini, A. ed. International Atomic Energy Agency (IAEA) (2001)
21. P. Archier, C. De Saint Jean, G. Noguere, J. Tommasi, J. Kor. Phys. Soc. **59**, 915 (2011)
22. A. Yu. Konobeyev, U. Fischer, S.P. Simakov, Nuc. Eng. Techn. **51**, 170 (2019)
23. A. Lépine-Szily, W. Sciani, Y.K. Watari, W. Mittig et al., Phys. Lett. B **304**, 45 (1993)
24. A. Lépine-Szily, M.S. Hussein, R. Lichtenthaler, J. Cseh, G. Lévai, Phys. Rev. Lett. **82**, 3972 (1999)
25. Wagner Sciani, Yul Otani, Alinka Lépine-Szily et al., Phys. Rev. C **80**, 034319 (2009)
26. J. Raynal, Report IAEA-SMR 9/8 (1988)
27. G.R. Satchler, Phys. Rep. **199**, 147 (1991)
28. R. Lichtenthäler Jr., A. Lépine-Szily, A.C.C. Villari, W. Mittig et al., Phys. Rev. C **26**, 2487 (1982)
29. L.F. Canto, R. Donangelo, M.S. Hussein, A. Lépine-Szily, Phys. Rev. Lett. **51**, 95 (1983)
30. R. Lichtenthäler Filho, A. Lépine-Szily, A.C.C. Villari, O. Portezan, Phys. Rev. C **39**, 884 (1989)
31. A. Lépine-Szily, M.M. Obuti, R. Lichtenthäler Filho, J.M. Oliveira et al., Phys. Lett. B **243**, 23 (1990)
32. A. Lépine-Szily, R. Lichtenthäler Filho, M.M. Obuti, J.M. Oliveira et al., Phys. Rev. C **40**, 681 (1989)
33. D. Dehnhard, V. Shkolnik, M.A. Franey, Phys. Rev. Lett. **40**, 1549 (1978)
34. P.D. Kunz, Dwuck4/Dwuck5 University of Colorado, Internal report 535-613 (2019)
35. R.M. DeVries, LOLA, a DWBA program, University of Rochester, unpublished (2019)

36. P.D. Kunz, E. Rost, The Distorted-Wave Born Approximation, in *Computational Nuclear Physics 2*. ed. by K. Langanke, J.A. Maruhn, S.E. Koonin (Springer, New York, NY, 1993)
37. M.H. Macfarlane, S.C. Pieper, Ptolemy: a program for heavy-ion direct-reaction calculations (ANL–76-11(Rev1)). United States (1978)
38. P.D. Kunz Chuck, A Coupled Channels Code, The Niels Bohr Institute Computer Program Library (1977)
39. I.J. Thompson, Coupled reaction channels calculations in nuclear physics. Comput. Phys. Rep. **7**, 167 (1988). https://doi.org/10.1016/0167-7977(88)90005-6
40. M. Assunção, R. Lichtenthäler, V. Guimarães, A. Lépine-Szily, G.F. Lima, A.M. Moro, Phys. Rev. C **70**, 054601 (2004)
41. I. Tanihata, H. Hamagaki, O. Hashimoto, Y. Shida, N. Yoshikawa, K. Sugimoto, O. Yamakawa, T. Kobayashi, Phys. Rev. Lett. **55**, 2676 (1985)
42. T. Kobayashi, O. Yamakawa, K. Sugimoto, T. Shimoda, N. Takahashi, I. Tanihata, Phys. Rev. Lett. **60**, 2599 (1988)
43. G. Ryckewaert, J.M. Colson, M. Gaelens, M. Loiselet, N.Postiau, Nucl. Phys. A **701**, 323c (2002)
44. Twinsol: A dual superconducting solenoid system for low-energy radioactive nuclear beam research AIP Conference Proceedings. University of Notre Dame, USA **392**, 397 (1997). https://doi.org/10.1063/1.52712
45. N. Austern, Y. Iseri, M. Kamimura, M. Kawai, G. Rawitscher, M. Yahiro, Continuum discretized coupled-channels calculations for three-body models of deuteron-nucleus reactions. Phys. Rep. (Rev. Sect. Phys. Lett.) **154**, 125 (1987)
46. Y. Hirabayashi, Y. Sakuragi, Phys. Rev. Lett. **69**, 1892 (1992)
47. C. Samanta, Y. Sakuragi, M. Ito, M. Fujiwara, J. Phys. G: Nucl. Part. Phys. **23**, 1697 (1997)
48. N. Keeley, K. Rusek, Phys. Lett. B **375**, 9 (1996)
49. C. Signorini, A. Edifizi, M. Mazzocco, M. Lunardon, D. Fabris, A. Vitturi, P. Scopel et al., Phys. Rev. C **67**, 044607 (2003)
50. A. Pakou, N. Alamanos, N.M. Clarke, N.J. Davis et al., Phys. Lett. B **633**, 691 (2006)
51. A. Pakou, N. Alamanos, A. Gillibert, M. Kokkoris et al., Phys. Rev. Lett. **90**, 202701 (2003)
52. K. Zerva, A. Pakou, K. Rusek, N. Patronis et al., Phys. Rev. C **82**, 044607 (2010)
53. E.A. Benjamim, A. Lépine-Szily, D.R. Mendes Junior, R. Lichtenthäler et al., Phys. Lett. B **647**, 30 (2007)
54. A. Lépine-Szily, R. Lichtenthäler, V. Guimarães, Eur. Phys. J. **50**, 128 (2014)
55. L.C. Chamon, B.V. Carlson, L.R. Gasques, D. Pereira et al., Phys. Rev. C **66**, 014610 (2002)
56. N. Keeley, R. Raabe, N. Alamanos, J.L. Sida, Prog. Part. Nucl. Phys. **59**, 579 (2007)
57. V. Lapoux, N. Alamanos, F. Auger, V. Fekou-Youmbi, A. Gillibert, F. Marie, S. Ottini-Hustache, J.-L. Sida, Phys. Rev. C **66**, 034608 (2002)
58. M. Takashina, S. Takagi, Y. Sakuragi, Y. Iseri, Phys. Rev. C **67**, 037601 (2003)
59. M.E. Brandan, G.R. Satchler, Phys. Rep. **285**, 143 (1997)
60. N. Keeley, N. Alamanos, K.W. Kemper, K. Rusek, Prog. Part. Nuc. Phys. **63**, 396 (2009)
61. O.R. Kakuee, J. Rahighi, A.M. Sánchez-Benítez et al., Nucl. Phys. A **728**, 339 (2003)
62. K. Rusek, N. Keeley, K.W. Kemper, R. Raabe, Phys. Rev. C **67**, 041604 (2003)
63. K. Rusek, I. Martel, J. Gómez-Camacho, A.M. Moro, R. Raabe, Phys. Rev. C **72**, 037603 (2005)
64. L. Acosta, A.M. Sanchez-Benitez, I. Martel et al., Phys. Rev. C **84**, 044604 (2011)
65. A. di Pietro, G. Randisi, V. Scuderi, L. Acosta et al., Phys. Rev. Lett. **105**, 022701 (2010)
66. M. Cubero, J.P. Fernández-García, M. Rodriguez-Gallardo, L. Acosta et al., Phys. Rev. Lett. **109**, 262701 (2012)
67. V. Pesudo, M.J.G. Borge, A.M. Moro, J.A. Lay et al., Phys. Rev. Lett. **118**, 152502 (2017)
68. F.F. Duan, Y.Y. Yang, K. Wang, A.M. Moro, V. Guimarães et al., Phys. Lett. B **811**, 135942 (2020)
69. B.T. Kim, Phys. Lett. B **80**, 353 (1979)
70. U. Arlt, R. Bass, V. Hartmann, R. Renfordt, K. Sapotta, P. Fröbrich, W. Schäfer, Phys. Rev. C **22**(4), 1790 (1980)
71. E.F. Aguilera, J.J. Kolata, F.M. Nunes, F.D. Becchetti et al., Phys. Rev. Lett. **84**, 5058 (2000)
72. P.N. de Faria, R. Lichtenthäler, K.C.C. Pires, A.M. Moro, A. Lépine-Szily et al., Phys. Rev. C **82**, 034602 (2010)
73. S. Appannababu, R. Lichtenthäler, M.A.G. Alvarez, M. Rodríguez-Gallardo, A. Lépine-Szily et al., Phys. Rev. C **99**, 014601 (2019)
74. D. Escrig, A.M. Sanchez-Benitez, A.M. Moro, M.A.G. Alvarez, M.V. Andres et al., Nucl. Phys. A **792**, 2 (2007)
75. J.P. Fernández García, M. Cubero, M. Rodríguez-Gallardo, L. Acosta et al., Phys. Rev. Lett **110**, 142701 (2013)
76. V. Guimarães, J.J. Kolata, D. Peterson, P. Santi et al., Phys. Rev. Lett. **84**, 1862 (2000)
77. F.M. Nunes, I.J. Thompson, Phys. Rev. C **59**, 2652 (1999)
78. T. Matsumoto, T. Egami, K. Ogata, Y. Iseri, M. Kamimura, M. Yahiro, Phys. Rev. C **73**, 051602(R) (2006)
79. M. Rodríguez-Gallardo, J.M. Arias, J. Gómez-Camacho, R.C. Johnson, A.M. Moro, I.J. Thompson, J.A. Tostevin, Phys. Rev. C **77**, 064609 (2008)
80. M. Rodríguez-Gallardo, J.M. Arias, J. Gómez-Camacho, A.M. Moro, I.J. Thompson, J.A. Tostevin, Phys. Rev. C **80**, 051601(R) (2009)
81. R. Lichtenthäler, A. Lépine-Szily, V. Guimarães et al., Eur. Phys. J. A **25**, 733 (2005)
82. R. Lichtenthäler, M.A.G. Alvarez, A. Lépine-Szily, S. Appannababu, K.C.C. Pires et al., Few-Body Syst. **57**, 157 (2016)
83. P.N. de Faria, R. Lichtenthäler, K.C.C. Pires, A.M. Moro, A. Lépine-Szily et al., Phys. Rev. C **81**, 044605 (2010)
84. K.C.C. Pires, R. Lichtenthäler, A. Lépine-Szily, V. Guimarães, P.N. de Faria et al., Phys. Rev. C **83**, 064603 (2011)
85. K.C.C. Pires, R. Lichtenthäler, A. Lépine-Szily, V. Morcelle, Phys. Rev. C **90**, 027605 (2014)
86. V. Morcelle, R. Lichtenthäler, A. Lépine-Szily, V. Guimarães, K.C.C. Pires et al., Phys. Rev. C **95**, 014615 (2017)
87. V. Morcelle, R. Lichtenthäler, R. Linares, M.C. Morais, V. Guimarães et al., Phys. Rev. C **89**, 044611 (2014)
88. P.R.S. Gomes, J. Lubian, I. Padron, R.M. Anjos, Phys. Rev. C **71**, 017601 (2005)
89. J.M.B. Shorto, P.R.S. Gomes, J. Lubian, L.F. Canto et al., Phys. Lett. B **678**, 77 (2009)
90. A.S. Freitas, L. Marques, X.X. Zhang, M.A. Luzio, P. Guillaumon, R. Pampa Condori, R. Lichtenthäler, Braz. J. Phys. **46**, 120 (2016)
91. K.C.C. Pires, S. Appannababu, R. Lichtenthäler, O.C.B. Santos, Phys. Rev. C **98**, 014614 (2018)
92. V. Morcelle, K.C.C. Pires, M. Rodríguez-Gallardo, R. Lichtenthäler, A. Lépine-Szily et al., Phys. Lett. B **732**, 228 (2014)
93. J.P. Bychowski, P.A. DeYoung, B.B. Hilldore, J.D. Hinnefeld et al., Phys. Lett. B **596**, 26 (2004)
94. D.M. Brink, Phys. Lett. **40B**, 37 (1972)